Published online 18 July 2012

Nucleic Acids Research, 2012, Vol. 40, No. 18 ***9369–9378***
doi:10.1093/nar/gks668

Three-dimensionally designed protein-responsive RNA devices for cell signaling regulation

Shunnichi Kashida[1], Tan Inoue[1,2,*] and Hirohide Saito[2,3,4,*]

[1]Laboratory of Gene Biodynamics, Graduate School of Biostudies, Kyoto University, Oiwake-cho, Kitashirakawa, Sakyo-ku, Kyoto 606-8502, [2]International Cooperative Research Project (ICORP), Japan Science and Technology Agency (JST), 5 Sanban-cho, Chiyoda-ku, Tokyo 102-0075, [3]The Hakubi Center for Advanced Research and [4]Center for iPS Cell Research and Application (CiRA), Kyoto University, Kyoto 606-8507, Japan

Received March 21, 2012; Revised June 17, 2012; Accepted June 18, 2012

ABSTRACT

The three-dimensional (3D) structures of many biomacromolecules have been solved to reveal the functions of these molecules. However, these 3D structures have rarely been applied to constructing efficient molecular devices that function in living cells. Here, we demonstrate a 3D structure-based molecular design principle for constructing short hairpin RNA (shRNA)-mediated genetic information converters; these converters respond to specific proteins and trigger the desired gene expression by modulating the function of the RNA-processing enzyme Dicer. The inhibitory effect on Dicer cleavage against the shRNA designed to specifically bind to U1A spliceosomal protein was correlated with the degree of steric hindrance between Dicer and the shRNA-protein complex *in vitro*: The level of the hindrance was predicted based on the models. Moreover, the regulation of gene expression was achieved by using the shRNA converters designed to bind to the target U1A or nuclear factor-κB (NF-κB) p50 proteins expressed in human cells. The 3D molecular design approach is widely applicable for developing new devices in synthetic biology.

INTRODUCTION

Artificial signal-converting systems have the potential to respond to intracellular biomacromolecules (e.g. specific proteins) and can control and rewire gene networks in living cells (1–4). These systems could be useful devices in biological science, medical science and engineering. Generally, synthetic molecular devices have been designed by connecting naturally occurring modular parts [e.g. deoxyribonucleic acid (DNA), ribonucleic acid (RNA) and amino acid sequences] (5,6). Thus far, the method for constructing these devices depends on the primary and secondary structures of the biomolecules, without accounting for their three-dimensional (3D) structures. For example, several synthetic RNA devices that control gene expression through the interaction between RNA and its ligands (e.g. antibiotics or proteins) have been designed and constructed (1,2,7–10). Specific target-sensing sites (e.g. naturally occurring RNA motifs or *in vitro* selected RNA aptamers) were inserted into RNA sequences based on the free energies of the RNA secondary structures (11–13). However, the capabilities of such devices are difficult to predict in most cases. Another approach has been to use experimental evolution techniques to generate the functions of the RNA devices (14,15). These techniques are labor intensive in general, and it is impossible to predict whether the desired sequences are present in an RNA pool consisting of random sequences before evolution. Consequently, it has been impossible to predict or optimize the performance of the devices without performing a functional screen (14,15).

As a new approach to constructing predictable and functional devices, 3D molecular design incorporating tertiary interactions between the biomacromolecular components of the device now seems to be feasible because of the increasing number of molecular complexes in the 3D structure-based library. 3D design of biomacromolecular complexes is likely to serve as an advanced method for producing next generation devices in synthetic and chemical biology because the performance of such devices is highly predictable. However, a rational 3D design has not yet been implemented for constructing useful biomacromolecular complexes [e.g. RNA–protein complexes (RNP)] that function in living cells (11,16,17).

Naturally occurring RNA-mediated signal converters have been discovered in human systems (18–21). For example, the Lin28 protein interacts with pre-*let-7* microRNA (miRNA) and blocks the processing of

*To whom correspondence should be addressed. Tel: +81 75 366 7029; Fax: +81 75 366 7096; Email: hirohide.saito@cira.kyoto-u.ac.jp
Correspondence may also be addressed to Tan Inoue. Tel: +81 75 753 3997; Fax: +81 75 753 3996; Email: tan@kuchem.kyoto-u.ac.jp

pre-*let-7* miRNA into mature let-7 miRNA, which leads to the derepression of *let-7* target genes, including oncogenes and cell cycle genes. Crystal and nuclear magnetic resonance structural analyses have shown that the cooperative interactions of two distinct regions in the lin28-*let-7* complex are critical for inhibiting the activity of the RNA-processing enzyme Dicer (22). Accordingly, by mimicking the function of natural RNAs, we sought to construct a synthetic short hairpin RNA (shRNA) that responds to a protein of interest and activates target gene expression.

Here, we report the 3D structure-based molecular design and construction of RNA-mediated protein information converters. The RNA device is designed to interact with a target protein that is expressed in cells and trigger the desired gene expression. We designed protein-responsive shRNAs *in silico* on the basis of high-resolution structures of known RNP complexes and evaluated their performance in mammalian cells. The designed shRNA senses the target proteins and inhibits the activity of Dicer, thereby controlling the RNA interference (RNAi) pathway in a predictable manner.

MATERIALS AND METHODS

3D modeling of protein responsive shRNAs and their trigger proteins

The 3D atomic model of the N-terminal domain of U1A (human) and its binding motif in U1snRNA ($U1A_1$ motif) or in the 3′-untranslated region of U1A messenger RNA (mRNA; $U1A_2$ motif) were obtained from Protein Data Bank (PDB) (ID: 1URN and ID: 1AUD, respectively). The 3D atomic model of p50 [mouse nuclear factor-κB (NF-κB)] bound to its aptamer RNA was obtained from PDB (ID: 1OOA). The 3D model of human NF-κB p50 and its aptamer has yet to be determined; therefore, we used the model of mouse NF-κB p50 for our 3D design. Beforehand, we verified the amino acid sequence differences between mouse and human p50 and confirmed that the six point mutations between the two were on either the terminal region or the loop far from the RNA-binding domain; therefore, the mutations are likely not critical for the structure and binding affinity. Molecular designs were performed with Discovery Studio (Accelrys) as previously described (23). Parts of the protein sequences were trimmed *in silico* to correspond to the regions of p50 and U1A-expressing proteins. The RNA stem region of the p50 aptamer and U1A-binding motifs were connected to double-stranded RNA (dsRNA) by using the superimpose protocol. The corresponding atomic coordinates of sugar, base and phosphate backbone in the four terminal bp of dsRNA and the protein-binding RNA motif were tethered, and the distance between these tethered coordinates was minimized using least squares approximation polynomial.

shRNA transcription *in vitro*

For *in vitro* shRNA transcription, a single-stranded template was annealed to the T7 annealing primer 5′-GCTAA TACGACTCACTATA-3′. shRNAs were transcribed and purified as follows: the transcription reaction mixtures were incubated for 3–4 h at 37°C. Then, the template DNA was degraded for 20 min at 37°C with 10 µl of TURBO DNase (Ambion). Any proteins in the mixture were removed by phenol–chloroform extraction, and nucleotide monomers were removed by PD-10 column purification (GE Healthcare) and ethanol precipitation. The shRNAs were purified using 15% native polyacrylamide gel electrophoresis and eluted with 500 µl of elution buffer (0.5 M NaCl, 0.1% sodium dodecyl sulphate and 1 mM EDTA) at 37°C overnight. The eluted shRNAs were filtered with a 22-µm microfilter (Millex GP) and precipitated with ethanol. The DNA templates used in this study are described in Supplementary Table S2.

Inhibition assay of human Dicer cleavage for shRNA *in vitro*

In vitro-transcribed U1A protein-responsive shRNA device variants ($U1A_1$- or $dU1A_1$- sh 21–31; 0.5 µM) and recombinant U1A protein (0 or 5 µM) were mixed with 1 µl of 10 mM adenosine triphosphate (ATP), 0.5 µl of 50 mM $MgCl_2$, 4 µl of Dicer Reaction Buffer (Genlantis), 1 µl of 0.5 unit/µl Recombinant Human Dicer Enzyme (Genlantis) and water (up to 10 µl). The mixtures were incubated at 37°C for 15 h, and the incubation was stopped using 1 µl of Dicer stop solution. The mixtures were separated by 15% native polyacrylamide gel electrophoresis at 4°C for 30 min, and the gel was stained with SYBER-Green I and II (Takara Bio Inc). The fluorescence of the stained RNA was detected by FLA-7000 (Fujifilm). The assays using other samples were conducted using the above mentioned procedure.

Construction of NF-κB (p50), U1A or MS2 coat protein expression plasmids

The NF-κB p50 (amino acids 39–352 of human NF-κB1) gene was amplified by polymerase chain reaction from total complementary DNA (cDNA) from HeLa cells, using the following primers: NF-κB (p50) Fwd (5′-CCA GGATCCCACCATGGATGGCCCATACCTTCAAAT ATTAGAGC-3′) and NF-κB (p50) Rev (5′-tcgCTCGAG TTCAGGATAGTAGAGGAAAGGTTTTGG-3′). The gene was then cloned into pcDNA3.1-mycHisA (pcDNA, Invitrogen) between the BamHI and XhoI sites to construct the p50 expression plasmid, and the sequence was verified.

The sequence coding U1A (amino acids 2–98 of human U1A, without nuclear localization signal) or MS2 (bacteriophage MS2 coat protein with amino acids 68–81 deleted) was amplified using the following primers: U1A_T Fwd (5′-GACACCATGGGATCCGCAGTTCC CGAGA -3′)/U1A_T Rev (5′-TATGAGATCTTTTCAT CTTGGCAATGATATCTG-3′) or MS2-CP Fwd (5′-CA CCATGGGATCCGCTTCTAACTTTACTCAGTTCGT TCTC-3′)/MS2-CP Rev (5′-TATGAGATCTGTAGATG CCGGAGTTGGC-3′) from human U1A or MS2-GFP expression plasmids, respectively. In short, the U1A or MS2 expression plasmid was cloned into pcDNA5-mycHisA (pcDNA, Invitrogen) containing an Internal

Ribosomal Entry Site-(IRES)-driven DsRed-Express expression cassette from pIRES2-DsRed-Express (Clontech Laboratories, Mountain View, CA, USA) to construct the U1A or MS2 expression plasmid, and the sequence was verified.

EGFP expression control of the devices in cultured cells

The oligo sequences for constructing the shRNA expression plasmids are shown in (Supplementary Table S1). To assess the p50-responsive shRNAs (p50- or dp50-sh 22–28), 293FT cells (1.5×10^5 per well) grown for one day in 24-well plates were co-transfected with 0.3 μg of one of the following: p50- or dp50-sh 22–28 expression plasmid, 0.3 μg p50 or MS2 expression plasmid and Enhanced Green Fluorescent Protein (EGFP) expression plasmid using 2 μl of Lipofectamine 2000 (Invitrogen). To assess the U1A-responsive shRNAs, we used the corresponding shRNA-expressing plasmid instead of p50-sh 22–28. Twenty-four hours after transfection, following fluorescent microscopic analysis, the cells were collected and resuspended in the medium, and the mean intensity of EGFP fluorescence was determined using a flow cytometer (FACSAria, BD Bioscience). To exclude abnormal cells, those cells whose Foward Scatter and Side Scatter signal scopes were identical to those of untreated 293FT cells were selected for the calculation of mean intensities, and 30 000 cells per each sample were analysed. To measure the EGFP signal, a 488-nm semiconductor laser beam and a 530/30-nm emission detector were used.

RESULTS

Design principle of protein-responsive shRNA devices

We chose to design shRNA structures because they contain a simple stem-loop structure and have been used as powerful tools to knock down desired genes through the RNAi pathway. Human Dicer recognizes shRNA at the end of its stem and cleaves it at approximately the 22nd nucleotide from the 3′ and/or 5′ end to produce a functional dsRNA for performing RNAi (24,25). Human Dicer does not discriminate according to the size and structure of the shRNA loop region during its processing; therefore, desired sequences can generally be incorporated into the loop region (26). We have previously constructed a synthetic shRNA by simply inserting a kink-turn RNA motif (Kt), which binds to the ribosomal protein L7Ae in *Archaeoglobus fulgidus* (2), into the shRNA loop region. L7Ae modulates the function of Dicer through its specific binding to the shRNA; however, it is unclear whether the protein-binding site is optimally set in the shRNA to maximize the steric hindrance to obstruct Dicer. To solve this problem, we took a 3D molecular design approach to constructing sophisticated protein-responsive shRNA devices. The ability of the RNA-binding protein to inhibit Dicer-mediated cleavage should directly determine the RNA device's efficiency of RNAi control because steric hindrance can be predicted from the 3D model of Dicer and the shRNA–protein complexes (schematic representation and corresponding 3D structure are shown in Figure 1A). Accordingly, the engineered shRNA with a specific protein-binding site was designed by adding bp between the double-stranded region and the loop to adjust the orientation and distance from the Dicer cleavage site (Figure 1B).

In the 3D model, we predicted the region that is required by human Dicer to cleave the shRNA based on the high-resolution X-ray structure of *Giardia* Dicer and a single-particle analysis of human Dicer using electron microscopy (27,28). Although the entire crystal structure of human Dicer has not been solved, previous structural studies have revealed that the regions responsible for nuclease activity of both human and *Giardia* Dicers are similar (27,29). Two structural models of human Dicer have been proposed by incorporating the *Giardia* Dicer crystal structure into the human Dicer electron microscopy map (27). A credible model from previous structural and biochemical studies indicates that a helicase domain is located adjacent to the RNaseIII domains (26,27). However, it has been reported that the disruption of the helicase domain maintains the stability and activity of human Dicer (30–32), indicating that the activity of human Dicer is not affected. Therefore, we did not account for the helicase domain in our 3D model.

3D molecular design of U1A-responsive shRNA devices

We designed a series of shRNA devices that respond to the expression of U1A (referred to as $U1A_1$-sh 21–31; Figure 2). U1A is one of the most abundantly expressed mRNA-processing and housekeeping proteins in mammalian cells (33). We used the U1A N-terminal domain (amino acids 2–98), which does not contain the region for nuclear localization signal (amino acids 100–144), indicating that the expressed U1A will be present in both the cytoplasm and nucleus. The $U1A_1$-sh 21–31 RNAs consist of a loop region containing an RNA motif for binding to U1A and 21–31 consecutive bp containing the target sequence for an mRNA-encoding EGFP (Supplementary Figure S1A). The engineered shRNAs were designed based on a specific RNP complex, which is U1A's N-terminal domain that is associated with the corresponding U1A-binding motif in human U1's small nuclear RNA stem-loop II, whose high-resolution 3D structure is known (34,35). We used a 3D modeling method to define the degree of steric hindrance between human Dicer and U1A to optimize the performance of the device (+U1A, Figure 2, Supplementary Movies S1 and S2). Thus, if U1A interfered with the region that is required for the Dicer's recognition, it is likely to cause inhibition of the Dicer function. Indeed, the steric hindrance between the Dicer and U1A (with $U1A_1$-sh 23–29) was observed, and then, the RNP complex of $U1A_1$-sh 30–31 exceeded the expected access region of Dicer in our *in silico* 3D modeling (Figure 2, Supplementary Movie S2).

Biochemical and in cell analyses of U1A-responsive shRNA devices

To confirm the prediction that was derived from the 3D modeling of the $U1A_1$-shRNA device, we investigated whether the *in vitro*-transcribed $U1A_1$-sh 21–31 and the

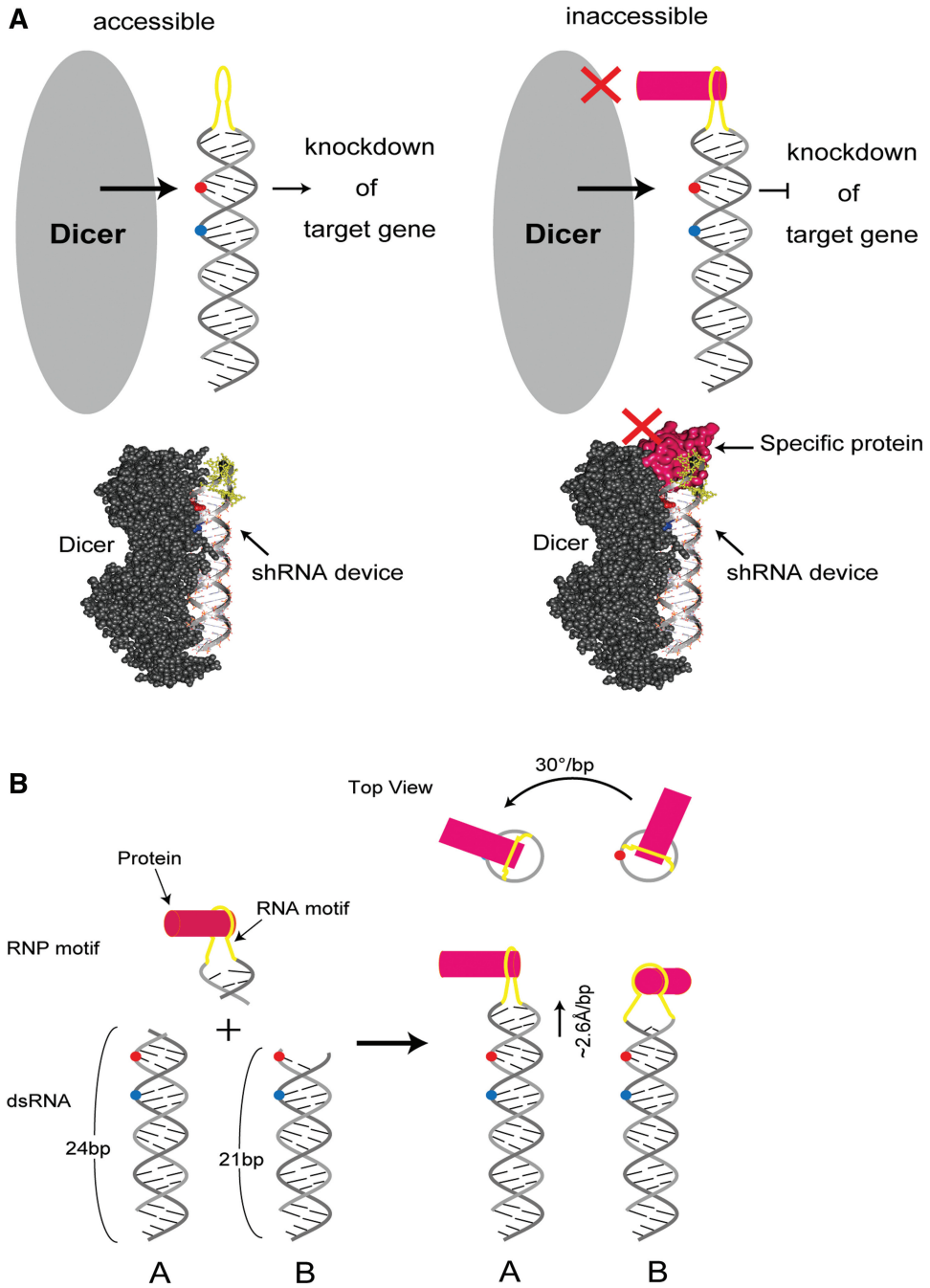

Figure 1. Schematic and structural model of the protein-responsive shRNA device mechanism and its bound protein orientation. (**A**) In the absence of the RNA-binding protein, the shRNA-processing enzyme Dicer (grey) can access and process the designed shRNA, and the processed shRNA induces the knockdown of its target gene through an RNAi mechanism (left). In contrast, Dicer is inaccessible to shRNA in the presence of a protein (pink) that binds to the loop region of the shRNA (yellow) because the RNP interaction faces Dicer and inhibits its access. The prevention of Dicer's function causes the derepression of the gene knockdown (right). (**B**) Protein-responsive shRNA devices A and B are designed by connecting an RNA–protein interaction motif with each length (A: 24 bp, B: 21 bp) of dsRNA. By specifying the position of two devices by reference to Dicer cleavage sites and comparing these two bound proteins' locations, we found that the protein bound on device A is located ~7.8 Å more distant to the Dicer cleavage sites and rotates ~90° in an anti-clockwise direction around the axis of the dsRNA compared with that bound on device B. Dicer cleavage sites are shown in two filled red and blue circles.

corresponding negative control, dU1A$_1$-sh 21–31, which contained a defective U1A binding motif (Supplementary Figure S1B), are processed by recombinant human Dicer in the presence or absence of U1A protein (Figure 3A and B and Supplementary Figure S2). In the absence of U1A, Dicer cleaved the transcribed U1A$_1$-sh 21–31 *in vitro*, which indicated that human Dicer can recognize and cleave the designed shRNAs containing the U1A-binding motif at the loop region (Figure 3A). As expected, the predicted effect of steric hindrance corresponded to the

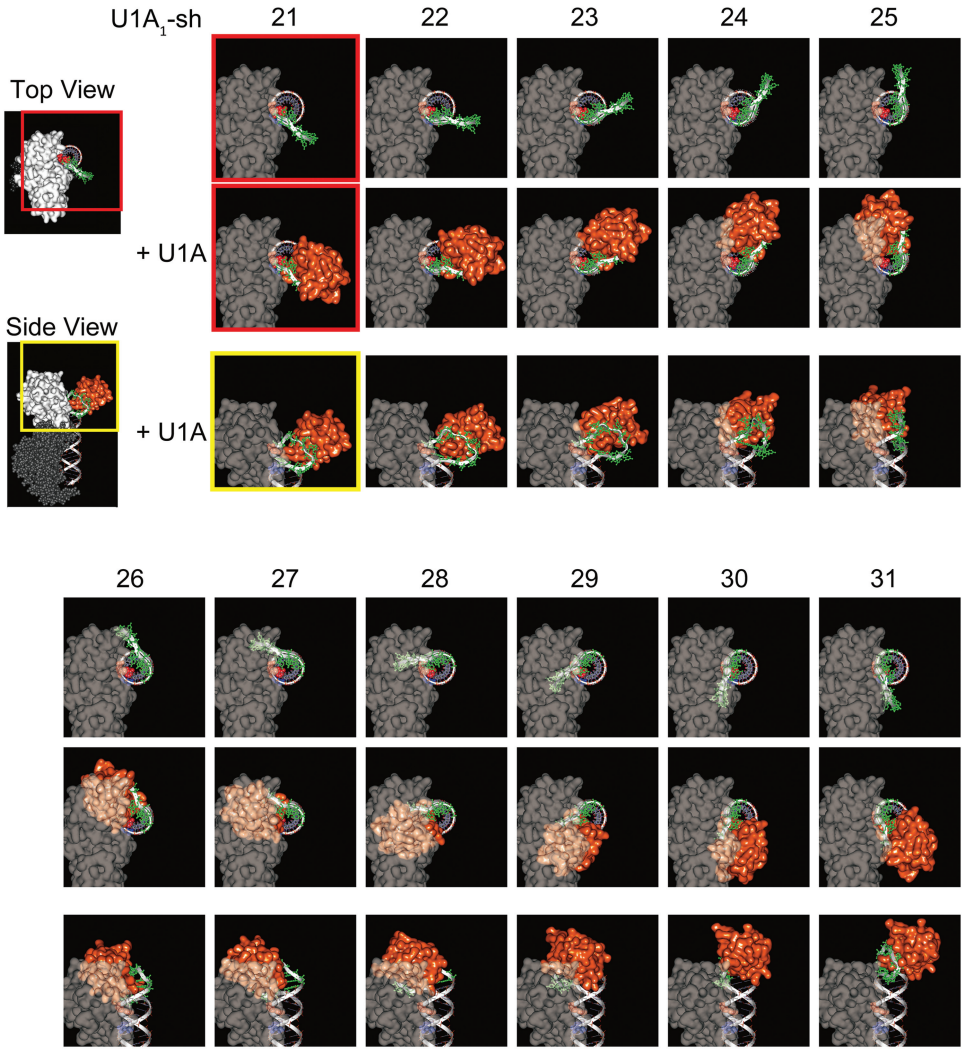

Figure 2. Predicted steric hindrance of U1A with Dicer in the 3D model of U1A-responsive shRNA devices. A 3D model of the catalytic domain and peripheral structure of *Giardia* Dicer (PDB ID: 2QVW, 326-385, 401- C-terminal amino acids), which is analogous to that of human Dicer, (white and white translucent) is displayed. Eleven U1A protein-responsive shRNA device variants, U1A$_1$-sh 21–31 (white ribbon) and bound U1A (orange) are shown. U1A$_1$-sh 21–31 consists of a loop region (green) that contains a U1A-binding motif with 21–31 bp of dsRNA targeting the EGFP gene. These models were arrayed with reference to the dsRNA axis and by producing two nucleotides (red spheres: 22nd nucleotide from the 5′ end and blue spheres: 22nd nucleotide from the 3′ end) that are located between the two metal ions of catalytic sites of *Giardia* Dicer. The expected accessing region of Dicer was indicated by a white translucent area.

degree of inhibition of the Dicer function in the presence of U1A (Figure 3A and B and Supplementary Figure S2B). Importantly, the U1A$_1$-sh 30–31 less efficiently inhibited Dicer cleavage when compared with U1A$_1$-sh 24–29, indicating that the longer stem in U1A$_1$-sh 30–31 can release the U1A-mediated inhibition of Dicer activity (Figure 3A and B). As anticipated, the result is consistent with the prediction based on the *in silico* models (Figure 2, sh30–31). We next investigated the cellular function of U1A$_1$-sh 21–25 because the inhibition efficiency of Dicer cleavage observed for U1A$_1$-sh 26–29 stays roughly constant. The designed U1A$_1$-sh 21–25 expression plasmids or the corresponding negative control dU1A$_1$-sh 21–25 expression plasmids were transfected into human cultured 293FT cells expressing U1A or the control bacteriophage MS2 coat protein. Twenty-four hours after transfection, the level of EGFP was measured with a flow cytometer. In the MS2-expressing cells, efficient down-regulation of EGFP expression was observed when U1A$_1$-sh 22–25 was transfected (red bars, Figure 3C). RNAi activity of U1A$_1$-sh 21 and dU1A$_1$-sh 21 was weaker than that of the other constructs (sh 22–25) (Figure 3C), indicating that the 21-bp length of the double-stranded region of the shRNAs is likely incompetent for Dicer processing in cell. The effective de-repression of EGFP expression when U1A$_1$-sh 25 was transfected into U1A-expressing cells was observed by flow cytometry (blue bars, Figure 3C and Supplementary Figure S3) and fluorescent microscopy (Figure 3D). The binding-defective shRNA expression plasmids (dU1A$_1$-sh 22–25) had no influence on RNAi activity *in vitro* Dicer cleavage assay (Supplementary Figure S2) and in cells expressing U1A (Figure 3C and Supplementary Figure S3), indicating that the

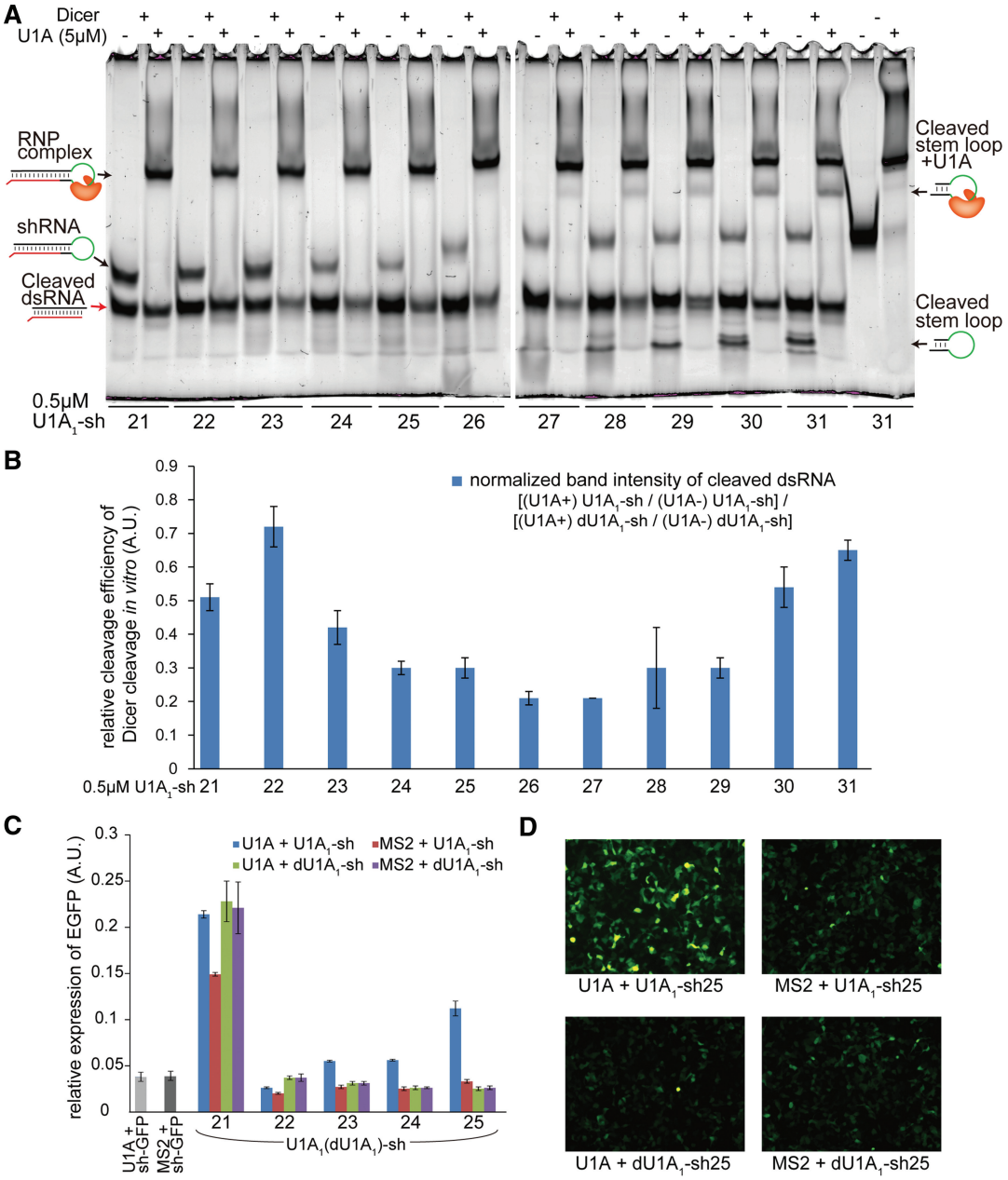

Figure 3. *In vitro* and cellular performance of U1A-responsive shRNA devices. (**A**) Human Dicer cleavage assay *in vitro*. $U1A_1$-sh 21–31 and U1A formed the RNP complex. $U1A_1$-sh 23–29 modulated Dicer activity in the presence of U1A. (**B**) The relative efficiency values of Dicer cleavage observed in (A) were calculated using the ratio of the cleaved band intensity in the presence of U1A to that in the absence of U1A and normalized to the value of $dU1A_1$-sh 21–31 (see also Supplementary Figure S2). (**C**) Flow cytometric analysis of the regulation of the RNA device variants by U1A in 293FT cells. 293FT cells were co-transfected with the three plasmids that expressed U1A or MS2, EGFP and one of the $U1A_1$- or $dU1A_1$-sh variants and were analysed the next day. The relative expression levels of EGFP fluorescence in the U1A- or MS2-expressing cells were normalized to the EGFP expression levels of the sh-N (negative control for EGFP knockdown, see Supplementary Table S1) and U1A- or MS2-expressing cells. The error bars indicate the standard deviations of three independent experiments. sh-GFP was used as a positive control for EGFP knockdown. (**D**) Fluorescent microscopic images of cells that expressed EGFP, $U1A_1$- or $dU1A_1$-sh 25 and U1A or MS2 from each plasmid.

RNA–protein interaction is responsible for suppressing RNAi activity. Thus, it is conceivable that the degree of steric hindrance between U1A and human Dicer is predictable from the 3D models. U1A located on the $U1A_1$-sh 25 effectively interfered with the Dicer accessible region (Figure 2 and Supplementary Movie S2). The effect of this steric hindrance observed in $U1A_1$-sh23–25-U1A complex models was positively correlated with the ability to de-repress EGFP expression in a phased manner (Figures 2 and 3 and Supplementary Figure S3).

3D molecular design and in cell analyses of p50-responsive shRNA devices

To confirm the versatility of the molecular design based on the 3D structure, we constructed a series of shRNA

devices that respond to the p50 domain of NF-κB (Figure 4A and Supplementary Movies S3 and S4). NF-κB is one of the major transcription factors in eukaryotic cells, and its abnormal expression has been linked to the proliferation of several types of tumor cells (36,37). The NF-κB-responsive shRNAs (referred to as p50-sh 22–28) consist of a loop region containing a specific binding site for p50 and a stem (22–28 bp), which contains the targeting sequence for an mRNA-coding EGFP (Figure 4A and Supplementary Figure S4A). The p50 domain consists of two parts: the N-terminal domain (p50-N, colored sky blue) and the C-terminal domain (p50-C, colored green; p50-N and p50-C are connected via a linker peptide in Figure 4A). The p50-N, but not the p50-C, domain tightly binds to the aptamer sequence inserted into the loop region of the shRNA (Figure 4A) (38,39). Notably, p50 does not contain a nuclear localization signal peptide; therefore, the expressed p50 will be present in the both the cytoplasm and nucleus.

The properties of the designed p50-sh 22–28 expression plasmids and the corresponding negative control dp50-sh 22–28 expression plasmids containing a defective p50 aptamer (Supplementary Figure S4B) were examined in 293FT cells that expressed p50 or MS2. In the MS2-expressing cells, a pronounced and moderate down-regulation of EGFP expression was observed when p50-sh 22–26 and p50-sh 27–28 expression plasmids were transfected, respectively (Figure 4B). *In vitro*-transcribed p50-sh 22–28 RNAs are processed by recombinant human Dicer in a similar manner (Supplementary Figure S5A and S5B). In the presence of p50, the down-regulation of EGFP was suppressed when p50-sh 26–28 expression plasmids were transfected (Figure 4B and C and Supplementary Figure S5C). The defective shRNAs (dp50-sh 22–28) that were incapable of binding to p50 had no influence on RNAi activity in cells expressing p50 (Figure 4B & Supplementary Figure S5C). It is conceivable that the degree of the steric hindrance between p50 and Dicer is predictable from the 3D models as in the case of U1A; p50 that is located on sh 26–28 effectively interferes with the Dicer accessible region (+p50, Figure 4A and Supplementary Movie S4).

3D design and cellular function of an alternative device with the protein-stabilized RNA structural motif

As an extension of this design, we constructed an alternative device with a more complex 3D RNP structure (Supplementary Figure S6). We attempted to inhibit Dicer function by using both an RNA-binding protein and the protein-stabilized RNA structural motif because

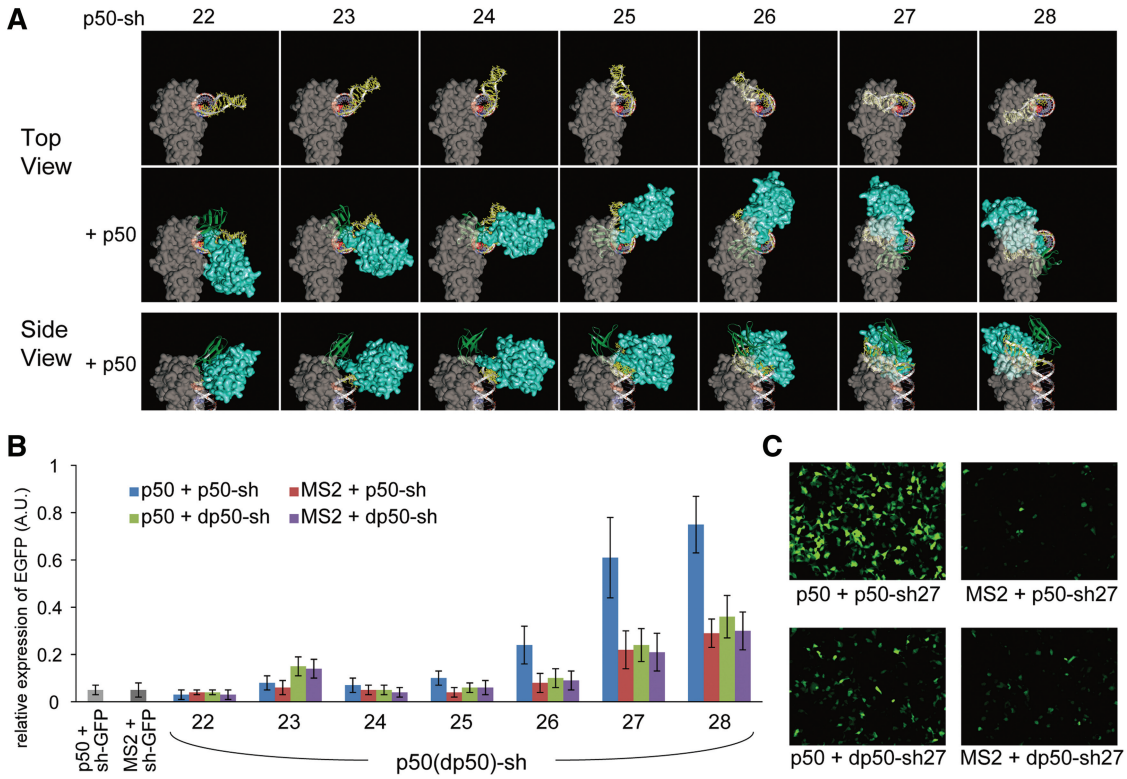

Figure 4. Prediction and assessment of the steric hindrance between Dicer and NF-κB p50 attached to p50-responsive shRNA devices. (**A**) The 3D model of seven p50 protein-responsive shRNA device variants, p50-sh 22–28 (white ribbon) and bound p50 (N-terminal domain with linker: sky blue; C-terminal domain: dark green). p50-sh 22–28 consists of the loop region (yellow) that contains an aptamer for p50 with 22–28 bp of dsRNA. These models were arrayed using the same procedure as shown in Figure 2. (**B**) Flow cytometric analysis of the regulation of the p50-sh variants by p50 expression in 293FT cells. 293FT cells were co-transfected with the three plasmids that expressed p50 or MS2, EGFP and one of the p50- or dp50-sh variants and were analysed the next day. The relative expression levels of EGFP fluorescence in the p50- or MS2-expressing cells were normalized to the EGFP expression levels of the sh-N and p50 or MS2 expressing cells. The error bars indicate the standard deviations of three independent experiments. sh-GFP was used as the positive control for EGFP knockdown. (**C**) Fluorescent microscopic images of cells that expressed EGFP, p50- or dp50-sh 27, and p50 or MS2 from each plasmid.

a certain RNA–protein interaction is known to stabilize the RNA structural motif containing the protein-binding site (40). Accordingly, we incorporated the U1A-binding RNA motif into the loop region that is flanked by the two RNA stems; the U1A-stabilized RNA structural motif presumably contributes to the effect of steric hindrance. The corresponding construct ($U1A_2$-sh 21–27) was designed to exhibit a loop-stem-loop structure (shown in green) and contains the U1A-binding motif that is connected to the main stem (21–27 bp; Supplementary Figure S6A) (33,40). The loop-stem-loop motif of $U1A_2$-sh is predicted to be more rigid than the loop structure of $U1A_1$-sh in terms of RNA secondary structure (40). The 3D model of the shRNA–U1A complex shows that the protruding portion of the RNA UUCG loop with the 5′-GUCC/GGAC-3′ stem region (which is referred to as the UUCG stem-loop) and U1A are arranged symmetrically (Supplementary Figure S6B). The steric hindrance between Dicer and U1A ($U1A_2$-sh 21 and $U1A_2$-sh 24–27) or between Dicer and the UUCG stem-loop that is bound to U1A ($U1A_2$-sh 21–24) can be seen in the 3D models.

To test the cellular function of the $U1A_2$-sh 21–27 RNA devices, we transfected the designed expression plasmids ($U1A_2$-sh 21–27 and d$U1A_2$-sh21–27; Supplementary Figure S6A) into 293FT cells that expressed either U1A or control MS2 (Supplementary Figure S7). The suppression of RNAi was observed when the $U1A_2$-sh 22–26 constructs were transfected into the U1A-expressing cells. We confirmed that the designed $U1A_2$-sh 24 interacted specifically with recombinant U1A and that the catalytic activity of Dicer was efficiently blocked by the RNP interaction *in vitro* (Supplementary Figure S8). U1A presumably stabilizes the conformation of the UUCG stem-loop region so that both the U1A-stabilized UUCG stem-loop region and U1A should become responsible for steric hindrance with Dicer (Supplementary Figure S6). Both $U1A_2$-sh 21 and $U1A_2$-sh 27 and their negative control plasmids induce RNAi weakly in the absence of U1A when compared with $U1A_2$-sh 22–26 and their negative control plasmids, indicating that the performance of the designed switches reflect a balance between the proper positioning of the U1A–shRNA complex to interfere with Dicer and the activity of the designed shRNA (without protein) to proceed in the correct RNAi pathway. In particular, both $U1A_2$-sh 27 and p50-sh 27–28 (and their negative control plasmids) with longer dsRNA region induce RNAi weakly in the absence of the corresponding protein compared with the other constructs with shorter dsRNA regions (Figure 4B and Supplementary Figure S7A). Thus, longer dsRNA region (>27 bp) of the shRNA seems incompetent for facilitating cellular RNAi pathway. Consequently, synthetic shRNAs with the proper lengths of dsRNA (22–27 bp) should be used for building a more diverse array of orthogonal devices: the range from 22 to 27 bp dsRNA is likely sufficient to generate the optimal shRNA devices. The 22–27 shRNAs can rotate the RNA motif ~150° (Figures 2 and 4A) so that the steric hindrance can be optimized within the range in most cases.

DISCUSSION

We have demonstrated that the 3D modeling of synthetic shRNAs and RNA-binding proteins is highly useful for developing efficient and tunable protein-responsive RNA devices; *in silico* 3D modeling predicted functional devices that control RNAi in mammalian cells. The designed protein-responsive shRNAs provide the proper orientation of the bound protein on the structured RNA loop for disturbing Dicer-dependent RNA cleavage activity in the 3D model.

For our 3D model of human Dicer, we referred to RNaseIII's catalytic domain and the peripheral structure of *Giardia* Dicer because structural studies have indicated that the crystal structure of *Giardia* Dicer is geometrically similar to the nuclease core of human Dicer (27,29). For our *in silico* 3D modeling, *in vitro* Dicer cleavage and cellular gene expression analyses indicated that there is a clear correlation between the model and our experimental data: The designed RNA devices can efficiently regulate the function of Dicer in human cells as in the case of the *in vitro* experiments, although we are unable to disregard the possibility that unexpected interactions between the RNP and some other molecules might affect the regulation of the shRNA devices in cells.

The introduction of a set of RNA devices that respond to multiple proteins could simultaneously and independently control multiple signals to improve the performance of synthetic signaling circuits in a single cell. For example, we have succeeded in re-directing apoptosis pathways of cultured human cells by using two distinct RNA devices that simultaneously regulate the expression of two apoptosis regulatory proteins (2). In addition, the RNA devices responding to endogenously produced proteins could rewire gene regulatory networks for therapeutic applications. For example, the *in vivo* systemic delivery systems of shRNA have been developed, although the precise delivery to the specific cells of interest remains unresolved (41). Our protein-responsive shRNA devices could be advantageous for controlling RNAi activity in the target cells because the function of synthetic shRNAs can be regulated depending on intracellular environment.

Precisely and strictly controllable RNA devices could be designed and developed based on the 3D structure by: (i) introducing multiple RNP interaction motifs into the appropriate region(s) of the shRNA device, (ii) altering the binding affinity and specificity to the sensing protein of interest or (iii) regulating the degree of steric hindrance between RNA and the corresponding RNA-binding proteins. Therefore, the 3D design of synthetic RNP-mediated information converters could contribute to the synthetic biology and other fields as a versatile tool for biomacromolecular design (9,16,17). This design principle can be applied to other biomacromolecular complexes (e.g. DNA–protein or protein–protein complexes) whose high-resolution 3D structures have already been solved. In addition, the 3D design strategies that are used to investigate the effects of steric hindrance between RNA and proteins on the function of RNA-processing enzymes could be useful for studying the relationship between the

molecular mechanisms and the structures of naturally occurring RNP complexes that are involved in RNA processing and/or regulation pathways (22,27).

SUPPLEMENTARY DATA

Supplementary Data are available at NAR Online: Supplementary Tables 1 and 2, Supplementary Figures 1–8, Supplementary Methods, Supplementary Movies 1–4 and Supplementary Reference [42].

ACKNOWLEDGEMENTS

The authors thank Y. Tomari (The University of Tokyo), Y. Fujita (Kyoto University) and Kei Endo (Kyoto University) for many helpful discussions. They also thank A. Hüttenhofer (Innsbruck Medical University), T. S. Rozhdestvensky (University of Muenster) and T. Ohtsuki (Okayama University) for providing the plasmids. S.K., T.I. and H.S. designed the project and evaluated the experimental results. S.K. performed 3D molecular design and experiments. S.K., T.I. and H.S. wrote the manuscript.

FUNDING

The International Cooperative Research Project (ICORP), Japan Science and Technology Agency (JST) (to T.I. and H.S.); the Takeda Science Foundation (to H.S.); the New Energy and Industrial Technology Development Organization [NEDO; 09A02021a to H.S.]; Japan Society for the Promotion of Science [Grants-in-Aid for JSPS Fellow, 22-6449 to S.K., Grant-in-Aid for Young Scientists (A) to H.S.]. Funding for open access charge: ICORP, JST.

Conflict of interest statement. None declared.

REFERENCES

1. Culler,S.J., Hoff,K.G. and Smolke,C.D. (2010) Reprogramming cellular behavior with RNA controllers responsive to endogenous proteins. *Science*, **330**, 1251–1255.
2. Saito,H., Fujita,Y., Kashida,S., Hayashi,K. and Inoue,T. (2011) Synthetic human cell fate regulation by protein-driven RNA switches. *Nat. Commun.*, **2**, 160.
3. Saito,H., Kobayashi,T., Hara,T., Fujita,Y., Hayashi,K., Furushima,R. and Inoue,T. (2010) Synthetic translational regulation by an L7Ae-kink-turn RNP switch. *Nat. Chem. Biol.*, **6**, 71–78.
4. Xie,Z., Wroblewska,L., Prochazka,L., Weiss,R. and Benenson,Y. (2011) Multi-input RNAi-based logic circuit for identification of specific cancer cells. *Science*, **333**, 1307–1311.
5. Canton,B., Labno,A. and Endy,D. (2008) Refinement and standardization of synthetic biological parts and devices. *Nat. Biotechnol.*, **26**, 787–793.
6. Deans,T.L., Cantor,C.R. and Collins,J.J. (2007) A tunable genetic switch based on RNAi and repressor proteins for regulating gene expression in mammalian cells. *Cell*, **130**, 363–372.
7. An,C.I., Trinh,V.B. and Yokobayashi,Y. (2006) Artificial control of gene expression in mammalian cells by modulating RNA interference through aptamer-small molecule interaction. *RNA*, **12**, 710–716.
8. Beisel,C.L., Bayer,T.S., Hoff,K.G. and Smolke,C.D. (2008) Model-guided design of ligand-regulated RNAi for programmable control of gene expression. *Mol. Syst. Biol.*, **4**, 224.
9. Isaacs,F.J., Dwyer,D.J. and Collins,J.J. (2006) RNA synthetic biology. *Nat. Biotechnol.*, **24**, 545–554.
10. Muller,M., Weigand,J.E., Weichenrieder,O. and Suess,B. (2006) Thermodynamic characterization of an engineered tetracycline-binding riboswitch. *Nucleic Acids Res.*, **34**, 2607–2617.
11. Beisel,C.L. and Smolke,C.D. (2009) Design principles for riboswitch function. *PLoS Comput. Biol.*, **5**, e1000363.
12. Ogawa,A. (2011) Rational design of artificial riboswitches based on ligand-dependent modulation of internal ribosome entry in wheat germ extract and their applications as label-free biosensors. *RNA*, **17**, 478–488.
13. Salis,H.M., Mirsky,E.A. and Voigt,C.A. (2009) Automated design of synthetic ribosome binding sites to control protein expression. *Nat. Biotechnol.*, **27**, 946–950.
14. Muranaka,N., Sharma,V., Nomura,Y. and Yokobayashi,Y. (2009) An efficient platform for genetic selection and screening of gene switches in Escherichia coli. *Nucleic Acids Res.*, **37**, e39.
15. Sinha,J., Reyes,S.J. and Gallivan,J.P. (2010) Reprogramming bacteria to seek and destroy an herbicide. *Nat. Chem. Biol.*, **6**, 464–470.
16. Liang,J.C., Bloom,R.J. and Smolke,C.D. (2011) Engineering biological systems with synthetic RNA molecules. *Mol. Cell.*, **43**, 915–926.
17. Saito,H. and Inoue,T. (2009) Synthetic biology with RNA motifs. *Int. J. Biochem. Cell Biol.*, **41**, 398–404.
18. Liu,G., Min,H., Yue,S. and Chen,C.-Z. (2008) Pre-miRNA loop nucleotides control the distinct activities of mir-181a-1 and mir-181c in early T cell development. *PLoS ONE*, **3**, e3592.
19. Michlewski,G. and Caceres,J.F. (2010) Antagonistic role of hnRNP A1 and KSRP in the regulation of let-7a biogenesis. *Nat. Struct. Mol. Biol.*, **17**, 1011–1018.
20. Ray,P.S., Jia,J., Yao,P., Majumder,M., Hatzoglou,M. and Fox,P.L. (2009) A stress-responsive RNA switch regulates VEGFA expression. *Nature*, **457**, 915–919.
21. Rybak,A., Fuchs,H., Smirnova,L., Brandt,C., Pohl,E.E., Nitsch,R. and Wulczyn,F.G. (2008) A feedback loop comprising lin-28 and let-7 controls pre-let-7 maturation during neural stem-cell commitment. *Nat. Cell. Biol.*, **10**, 987–993.
22. Nam,Y., Chen,C., Gregory,R.I., Chou,J.J. and Sliz,P. (2011) Molecular basis for interaction of let-7 MicroRNAs with Lin28. *Cell*, **147**, 1080–1091.
23. Ohno,H., Kobayashi,T., Kabata,R., Endo,K., Iwasa,T., Yoshimura,S.H., Takeyasu,K., Inoue,T. and Saito,H. (2011) Synthetic RNA-protein complex shaped like an equilateral triangle. *Nat. Nanotechnol.*, **6**, 116–120.
24. Park,J.-E., Heo,I., Tian,Y., Simanshu,D.K., Chang,H., Jee,D., Patel,D.J. and Kim,V.N. (2011) Dicer recognizes the 5′ end of RNA for efficient and accurate processing. *Nature*, **475**, 201–205.
25. Vermeulen,A., Behlen,L., Reynolds,A., Wolfson,A., Marshall,W.S., Karpilow,J. and Khvorova,A. (2005) The contributions of dsRNA structure to Dicer specificity and efficiency. *RNA*, **11**, 674–682.
26. Tsutsumi,A., Kawamata,T., Izumi,N., Seitz,H. and Tomari,Y. (2011) Recognition of the pre-miRNA structure by Drosophila Dicer-1. *Nat. Struct. Mol. Biol.*, **18**, 1153–1158.
27. Lau,P.W., Potter,C.S., Carragher,B. and MacRae,I.J. (2009) Structure of the human Dicer-TRBP complex by electron microscopy. *Structure*, **17**, 1326–1332.
28. Macrae,I.J., Zhou,K., Li,F., Repic,A., Brooks,A.N., Cande,W.Z., Adams,P.D. and Doudna,J.A. (2006) Structural basis for double-stranded RNA processing by Dicer. *Science*, **311**, 195–198.
29. Takeshita,D., Zenno,S., Lee,W.C., Nagata,K., Saigo,K. and Tanokura,M. (2007) Homodimeric structure and double-stranded RNA cleavage activity of the C-terminal RNase III domain of human dicer. *J. Mol. Biol.*, **374**, 106–120.
30. Lee,Y., Hur,I., Park,S.Y., Kim,Y.K., Suh,M.R. and Kim,V.N. (2006) The role of PACT in the RNA silencing pathway. *EMBO J.*, **25**, 522–532.
31. Ma,E., MacRae,I.J., Kirsch,J.F. and Doudna,J.A. (2008) Autoinhibition of human dicer by its internal helicase domain. *J. Mol. Biol.*, **380**, 237–243.

32. Macrae,I.J., Li,F., Zhou,K., Cande,W.Z. and Doudna,J.A. (2006) Structure of Dicer and mechanistic implications for RNAi. *Cold Spring Harb. Symp. Quant. Biol.*, **71**, 73–80.
33. van Gelder,C.W., Gunderson,S.I., Jansen,E.J., Boelens,W.C., Polycarpou-Schwarz,M., Mattaj,I.W. and van Venrooij,W.J. (1993) A complex secondary structure in U1A pre-mRNA that binds two molecules of U1A protein is required for regulation of polyadenylation. *EMBO J.*, **12**, 5191–5200.
34. Nagai,K., Oubridge,C., Ito,N., Avis,J. and Evans,P. (1995) The RNP domain: a sequence-specific RNA-binding domain involved in processing and transport of RNA. *Trends Biochem. Sci.*, **20**, 235–240.
35. Oubridge,C., Ito,N., Evans,P.R., Teo,C.H. and Nagai,K. (1994) Crystal structure at 1.92 A resolution of the RNA-binding domain of the U1A spliceosomal protein complexed with an RNA hairpin. *Nature*, **372**, 432–438.
36. Galardi,S., Mercatelli,N., Farace,M.G. and Ciafre,S.A. (2011) NF-kB and c-Jun induce the expression of the oncogenic miR-221 and miR-222 in prostate carcinoma and glioblastoma cells. *Nucleic Acids Res.*, **39**, 3892–3902.
37. Gaur,U. and Aggarwal,B.B. (2003) Regulation of proliferation, survival and apoptosis by members of the TNF superfamily. *Biochem. Pharmacol.*, **66**, 1403–1408.
38. Huang,D.B., Vu,D., Cassiday,L.A., Zimmerman,J.M., Maher,L.J. 3rd and Ghosh,G. (2003) Crystal structure of NF-kappaB (p50)2 complexed to a high-affinity RNA aptamer. *Proc. Natl. Acad. Sci. USA*, **100**, 9268–9273.
39. Lebruska,L.L., Maher,L.J. and 3rd. (1999) Selection and characterization of an RNA decoy for transcription factor NF-kappa B. *Biochemistry*, **38**, 3168–3174.
40. Allain,F.H., Howe,P.W., Neuhaus,D. and Varani,G. (1997) Structural basis of the RNA-binding specificity of human U1A protein. *EMBO J.*, **16**, 5764–5772.
41. Takeshita,F., Patrawala,L., Osaki,M., Takahashi,R.U., Yamamoto,Y., Kosaka,N., Kawamata,M., Kelnar,K., Bader,A.G., Brown,D. *et al.* (2010) Systemic delivery of synthetic microRNA-16 inhibits the growth of metastatic prostate tumors via downregulation of multiple cell-cycle genes. *Mol. Ther.*, **18**, 181–187.
42. Endoh,T., Sisido,M. and Ohtsuki,T. (2008) Cellular siRNA delivery mediated by a cell-permeant RNA-binding protein and photoinduced RNA interference. *Bioconjug. Chem.*, **19**, 1017–1024.